Smart Structures and Systems, *Vol. 16, No. 5 (2015) 937-960*
DOI: http://dx.doi.org/10.12989/sss.2015.16.5.937

Extracting parameters of TMD and primary structure from the combined system responses

Jer-Fu Wang[1a] and Chi-Chang Lin[*2]

[1]*921 Earthquake Museum of Taiwan, National Museum of Natural Science, Taichung, Taiwan 413, R.O.C.*
[2]*Department of Civil Engineering, National Chung Hsing University, Taichung, Taiwan 402, R.O.C.*

(Received September 3, 2014, Revised May 26, 2015, Accepted June 29, 2015)

Abstract. Tuned mass dampers (TMDs) have been a prevalent vibration control device for suppressing excessive vibration because of environmental loadings in contemporary tall buildings since the mid-1970s. A TMD must be tuned to the natural frequency of the primary structure to be effective. In practice, a TMD may be assembled in situ, simultaneously with the building construction. In such a situation, the respective dynamic properties of the TMD device and building cannot be identified to determine the tuning status of the TMD. For this purpose, a methodology was developed to obtain the parameters of the TMD and primary building on the basis of the eigenparameters of any two complex modes of the combined building–TMD system. The theory was derived in state-space to characterize the nonclassical damping feature of the system, and combined with a system identification technique to obtain the system eigenparameters using the acceleration measurements. The proposed procedure was first demonstrated using a numerical verification and then applied to real, experimental data of a large-scale building–TMD system. The results showed that the procedure is capable of identifying the respective parameters of the TMD and primary structure and is applicable in real implementations by using only the acceleration response measurements of the TMD and its located floor.

Keywords: tuned mass damper (TMD); passive control; energy dissipation device; building structure; system identification

1. Introduction

A tuned mass damper (TMD) is well-known for its pendulum-like dynamic feature that suppresses the resonance effect of structures. The TMD dates back to 1909, when Frahm (1911) invented a device for mitigating the vibrations of dynamic bodies. The TMD proposed by Frahm (1911) was an undamped single-degree-of-freedom system. Ormondroyd and Den Hartog (1928) then introduced damping to it and proposed an optimal design concept for TMDs under narrow-band, cyclic external loadings. Researchers, such as Hahnkamm (1932) and Brock (1946), extensively discussed the problems of optimal frequency and optimal damping of a TMD, which

∗Corresponding author, Distinguished Professor, E-mail: cclin3@dragon.nchu.edu.tw
[a] Assistant Research Fellow, E-mail: jfwang@mail.921emt.edu.tw

http://www.techno-press.org/?journal=sss&subpage=8 ISSN: 1738-1584 (Print), 1738-1991 (Online)

were thoroughly documented in a book by Den Hartog (1956).

TMDs have been applied to vibration control in buildings since the 1970s. The John Hancock Tower in Boston, Citicorp Center in New York City, and CN Tower in Toronto were the pioneering buildings and observatory towers equipped with this type of device against wind loads. Since then, numerous studies have been published (Wirsching and Campbell 1973, McNamara 1977, Luft 1979, Warburton 1982, Kwok 1984, Villaverde 1985, Lin *et al.* 1994), with most of them focusing on optimizing TMD parameters under sinusoidal force, white noise, or random excitation. In recent years, optimizing TMD parameters has remained a prevalent research topic with investigation having been conducted on asymmetry, soil-structure interaction, nonlinearity, uncertainty, and multistory building models (Ueng *et al.* 2008, Marano and Quaranta 2009, Wang *et al.* 2009, Marano *et al.* 2010a, b, Sgobba and Marano 2010, Bekdaş and Nigdeli 2011, Bisegna and Caruso 2011, Chakraborty and Roy 2011, Cheung and Wong 2011, Mohtat and Dehghan-Niri 2011, Steinbuch 2011, Almazán *et al.* 2012, Tigli 2012, Zilletti *et al.* 2012, Bekdaş and Nigdeli 2013, Farshidianfar and Soheili 2013, Greco and Marano 2013, Yu *et al.* 2013). In addition, on the basis of a single mass-damping-stiffness system, different types of TMD have been derived and adapted to different situations. For instance, Xu and Igusa (1992) proposed a multiple tuned mass damper (MTMD), in which the mass of a TMD is divided into separate units in parallel with different fundamental frequencies to form a broader frequency bandwidth. The MTMD has also been the focus of numerous studies (Kareem and Kline 1995, Jangid 1999, Li 2000, Park and Reed 2001, Bakre and Jangid 2004, Wang and Lin 2005, Li and Zhu 2006, Lin and Wang 2012). Other types of TMD, such as dual-TMD systems (Oka *et al.* 2009) and nonlinear TMDs (Alexander and Schilder 2009, Viguie and Kerschen 2009, Viguie and Kerschen 2010, Wang *et al.* 2010, Jangn *et al.* 2012), have been proposed for various situations.

Early practical successes and decades of continual developments in design theory have increased TMD installations in contemporary tall buildings and towers worldwide. The Burj Al Arab in Dubai, Highcliff in Hong Kong, Taipei 101 in Taiwan, Aspire Tower in Qatar, Canton Tower in China, Tokyo Skytree in Japan, and Shanghai Tower in China are all recent, real structures installed with TMDs. It is widely recognized that a TMD design requires prior knowledge of the controlled modal frequency, damping ratio, and mode shape of the primary structure. Moreover, a highly accurate modal frequency is required for achieving an optimal tuning condition between the TMD and primary structure. In practice, the following general procedure is used for designing and implementing a TMD: (1) System identification techniques are employed to obtain the modal parameters of the primary structure based on its response measurements. (2) The optimal TMD parameters are determined, and the device is then assembled. (3) The assembled TMD is tested and adjusted to ensure that its dynamic properties are as designed. (4) The TMD is installed in its designated location. However, for a new structure, it may be necessary to build the TMD concurrently with the construction of the primary structure, before the real dynamic parameters of the primary structure are identified. In such circumstances, the primary structure and TMD are combined. Neither the TMD nor the primary structure can be individually tested in situ. Therefore, it is necessary to develop a methodology for identifying the respective parameters of the TMD and structure to assure the effectiveness of the TMD control system.

Although an increasing number of real buildings are equipped with TMDs, detailed information about designing, assembling, installing, and testing TMDs has not been released to the public. In addition, the continuous monitoring of TMD-protected structures is a critical problem. Weber and Feltrin (2010) conducted forced- and random-vibration tests by using shakers on two TMD-protected pedestrian bridges that had been in service for 19 years. They simulated the

bridge–TMD system with a two-degrees-of-freedom model and found that one of the TMDs had become detuned since its installation. Brownjohn *et al.* (2010) investigated the performance of a TMD installed on the chimney of the Rugeley power station based on 1 year of data from its structural health-monitoring system. They employed the stochastic subspace identification (SSI) method for identifying the first two modal frequencies and modal damping ratios to evaluate the vibration reduction efficiency of the TMD. Recently, Shi *et al.* (2012) evaluated the dynamic properties of the ATMD combined system of the Shanghai World Financial Center building based on the field measurements of ATMD action from ambient-vibration and force-vibration tests. Li *et al.* (2011) analyzed the acceleration measurements of the Taipei 101 building during periods of several typhoons and the 2008 Wenchuan earthquake; however, the performance of the TMD was not discussed. More recently, Kang *et al.* (2012) examined TMD performance in the Poscoenc Tower building in Incheon, South Korea. A two-degrees-of-freedom model was used to simulate the TMD–building system, and an equation was derived to uncouple the natural frequencies of the TMD and building by using two modal frequencies of the combined system without considering damping.

In this study, a theoretical derivation in state–space and an analysis procedure were developed for extracting the modal parameters of a TMD and primary building from the acceleration responses of the TMD–building combined system. Both the natural frequency and damping ratio of the TMD and primary building were obtained. A multistory building with a TMD installed at an arbitrary floor was considered. The proposed analysis procedure consisted of two major parts: a newly developed parameter-extraction theory and system-identification techniques. The idea was to identify the complex eigenvalues and eigenvectors of the building–TMD system from seismic or ambient acceleration measurements and then to extract the respective modal parameters of the TMD and building on the basis of the identified eigenparameters. The proposed method was first demonstrated through numerical simulations and then validated using experimental data from shaking-table tests of a large-scale, three-story benchmark building equipped with an assembled TMD. Both the full and partial measurements of the acceleration responses were considered for examining the accuracy and applicability of the proposed method.

2. Theoretical development of the methodology

2.1 Equations of motion of the TMD–building system

For an *n*-story shear building with a TMD attached on the *l*th floor subjected to external excitations, as shown in Fig. 1, the equation of motion of the combined system can be written in matrix form as

$$\mathbf{M}\ddot{\mathbf{x}}(t)+\mathbf{C}\dot{\mathbf{x}}(t)+\mathbf{K}\mathbf{x}(t)=\mathbf{F}(t) \tag{1}$$

In Eq. (1), $\mathbf{M}$, $\mathbf{C}$, and $\mathbf{K}$ are the $N\times N$ (where $N=n+1$) mass, damping, and stiffness matrices, respectively, and can be expressed in detail as

$$\mathbf{M}=diag.[m_{p_1}\ \ m_{p_2}\ \ \ldots\ m_l\ \ \ldots\ m_{p_n}\ \ m_s] \tag{2}$$

$$\mathbf{C}=\begin{bmatrix} c_{p_1}+c_{p_2} & -c_{p_2} & 0 & \cdots & \cdots & \cdots & 0 \\ -c_{p_2} & c_{p_2}+c_{p_3} & -c_{p_3} & 0 & & & \vdots \\ 0 & \ddots & \ddots & \ddots & & & \vdots \\ \vdots & 0 & -c_{p_l} & c_{p_l}+c_{p_{l+1}}+c_s & -c_{p_{l+1}} & 0 & -c_s \\ \vdots & & \ddots & \ddots & \ddots & \vdots & \vdots \\ \vdots & & & 0 & -c_{p_n} & c_{p_n} & 0 \\ 0 & \cdots & \cdots & -c_s & \cdots & 0 & c_s \end{bmatrix} \tag{3}$$

$$\mathbf{K}=\begin{bmatrix} k_{p_1}+k_{p_2} & -k_{p_2} & 0 & \cdots & \cdots & \cdots & 0 \\ -k_{p_2} & k_{p_2}+k_{p_3} & -k_{p_3} & 0 & & & \vdots \\ 0 & \ddots & \ddots & \ddots & & & \vdots \\ \vdots & 0 & -k_{p_l} & k_{p_l}+k_{p_{l+1}}+k_s & -k_{p_{l+1}} & 0 & -k_s \\ \vdots & & \ddots & \ddots & \ddots & \vdots & \vdots \\ \vdots & & & 0 & -k_{p_n} & k_{p_n} & 0 \\ 0 & \cdots & \cdots & -k_s & \cdots & 0 & k_s \end{bmatrix} \tag{4}$$

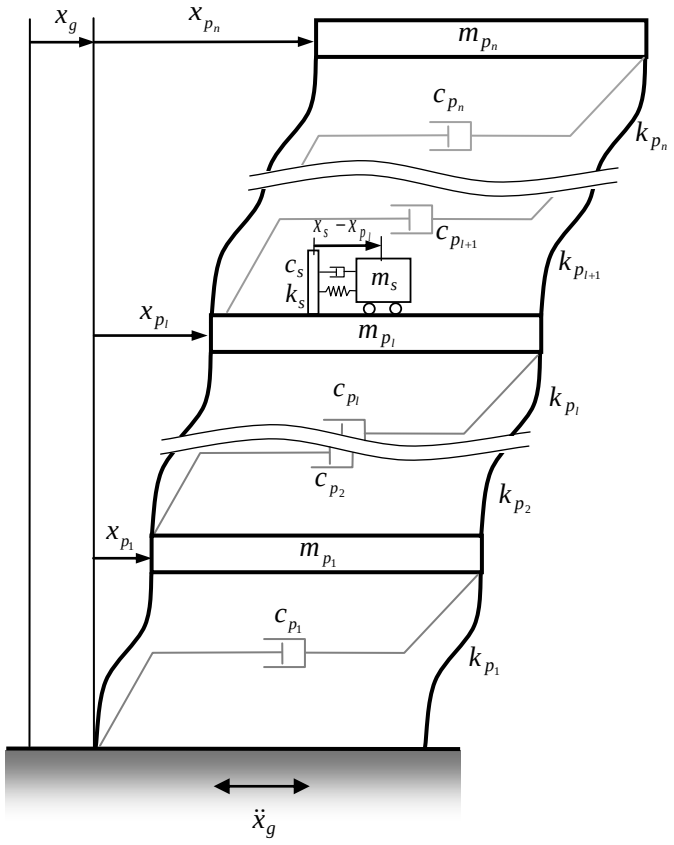

Fig. 1 System model of a multistory building structure with a tuned mass damper

where m_{p_i} and m_s represent the masses of the *i*th floor and TMD, respectively; c_{p_i} and c_s represent the damping coefficients of the *i*th story and TMD, respectively; and k_{p_i} and k_s denote the stiffness coefficients of the *i*th story and TMD, respectively. In addition, $\mathbf{x}=\{x_{p_1}\ x_{p_2}\ \ldots\ x_{p_i}\ \ldots\ x_{p_n}\ x_s\}^T$ is the $N\times 1$ displacement vector, where x_{p_i} and x_s represent the displacements of the *i*th floor and TMD relative to the ground, respectively. The notation $\mathbf{F}(t)$ represents the $N\times 1$ vector of external forces that can be wind, base excitations, or experimentally harmonic forces. In the situation of ground acceleration, $\ddot{x}_g(t)$, $\mathbf{F}(t)=\mathbf{M}\mathbf{r}\ddot{x}_g(t)$ where $\mathbf{r}=\{-1\ -1\ \ldots\ -1\ \ldots\ -1\ -1\}^T$ is the $N\times 1$ influence coefficient vector.

Equation (1) can be transformed into state–space form as follows

$$\dot{\mathbf{z}}(t)=\mathbf{A}\mathbf{z}(t)+\mathbf{B}\mathbf{F}(t) \tag{5}$$

where

$$\mathbf{A}=\begin{bmatrix}\mathbf{O} & \mathbf{I}\\ -\mathbf{M}^{-1}\mathbf{K} & -\mathbf{M}^{-1}\mathbf{C}\end{bmatrix},\ \mathbf{B}=\begin{Bmatrix}\mathbf{0}\\ \mathbf{M}^{-1}\end{Bmatrix} \tag{6}$$

and **z** is the state vector of $2N\times 1$ consisting of relative displacement and velocity responses; **A** represents the system matrix of the building–TMD system with a dimension of $2N\times 2N$; **I** is an identity matrix of $N\times N$; **O** is a zero matrix of $N\times N$; and **0** is a zero vector of $N\times 1$. The relationship between the state vector and an $m\times N$ output vector C_1 for the absolute acceleration of the system can be expressed using the following output equation

$$\mathbf{y}=C_1[-\mathbf{M}^{-1}\mathbf{K}\ -\mathbf{M}^{-1}\mathbf{C}]\,\mathbf{z} \tag{7}$$

where **y** is an $m\times 1$ output measurement vector with *m* sensors.

2.2 Identification of the natural frequency and damping ratio of the TMD

The terms λ_j and $\mathbf{\Psi}_j$ denote the *j*th eigenvalue and its corresponding $2N\times 1$ eigenvector of the system matrix **A**. The physical-domain system matrix is related to the *j*th eigenparameters by using the state–space characteristic equation:

$$(\mathbf{A}-\lambda_j\mathbf{I})\mathbf{\Psi}_j=\mathbf{0} \tag{8}$$

Substituting Eq. (6) into Eq. (8) gives

$$\left\{\begin{bmatrix}\mathbf{0} & \mathbf{I}\\ -\mathbf{M}^{-1}\mathbf{K} & -\mathbf{M}^{-1}\mathbf{C}\end{bmatrix}-\lambda_j\begin{bmatrix}\mathbf{I} & \mathbf{0}\\ \mathbf{0} & \mathbf{I}\end{bmatrix}\right\}\mathbf{\Psi}_j=\mathbf{0} \tag{9}$$

Furthermore, the expression of the lower half of Eq. (9), which contains information regarding the dynamic properties of the system, gives

$$\begin{bmatrix}\mathbf{L} & \mathbf{R}\end{bmatrix}\mathbf{\Psi}_j=\mathbf{0} \tag{10}$$

where

$$\mathbf{L}=\begin{bmatrix} -\frac{k_{p_1}+k_{p_2}}{m_{p_1}} & \frac{k_{p_2}}{m_{p_1}} & 0 & \cdots & \cdots & \cdots & 0 \\ \frac{k_{p_2}}{m_{p_2}} & -\frac{k_{p_2}+k_{p_3}}{m_{p_2}} & \frac{k_{p_3}}{m_{p_2}} & 0 & & \vdots & \vdots \\ 0 & \ddots & \ddots & \ddots & & \vdots & \vdots \\ \vdots & 0 & \frac{k_{p_l}}{m_{p_l}} & -\frac{k_{p_l}+k_{p_{l+1}}+k_s}{m_{p_l}} & \frac{k_{p_{l+1}}}{m_{p_l}} & \vdots & \frac{k_s}{m_{p_l}} \\ \vdots & \vdots & \ddots & \ddots & \ddots & \ddots & \vdots \\ \vdots & & \cdots & 0 & \frac{k_{p_n}}{m_{p_n}} & -\frac{k_{p_n}+k_s}{m_{p_n}} & 0 \\ 0 & \cdots & \cdots & \frac{k_s}{m_s} & \cdots & 0 & -\frac{k_s}{m_s} \end{bmatrix} \tag{11a}$$

$$\mathbf{R}=\begin{bmatrix} -\frac{c_{p_1}+c_{p_2}}{m_{p_1}}-\lambda_j & \frac{c_{p_2}}{m_{p_1}} & 0 & \cdots & \cdots & \cdots & 0 \\ \frac{c_{p_2}}{m_{p_2}} & -\frac{c_{p_2}+c_{p_3}}{m_{p_2}}-\lambda_j & \frac{c_{p_3}}{m_{p_2}} & 0 & & \vdots & \vdots \\ 0 & \ddots & \ddots & \ddots & & \vdots & \vdots \\ \vdots & 0 & \frac{c_{p_l}}{m_{p_l}} & -\frac{c_{p_l}+c_{p_{l+1}}+c_s}{m_{p_l}}-\lambda_j & \frac{c_{p_{l+1}}}{m_{p_l}} & \vdots & \frac{c_s}{m_{p_l}} \\ \vdots & \vdots & & \ddots & & & \vdots \\ \vdots & & \cdots & 0 & \frac{c_{p_n}}{m_{p_n}} & -\frac{c_{p_n}+c_s}{m_{p_n}}-\lambda_j & 0 \\ 0 & \cdots & \cdots & \frac{c_s}{m_s} & \cdots & 0 & -\frac{c_s}{m_s}-\lambda_j \end{bmatrix} \tag{11b}$$

$$\mathbf{\Psi}_j=\{\psi_{1j}\ \ \psi_{2j}\ \ \ldots\ \psi_{n,j}\ \ \psi_{N,j}\ \ \ldots\ \psi_{2N-1,j}\ \ \psi_{2N,j}\}^T \tag{12}$$

Both λ_j and the entries of $\mathbf{\Psi}_j$ are complex for an underdamped vibration system. The *j*th complex eigenvector can also be rewritten as $\mathbf{\Psi}_j=\{\mathbf{\Phi}_j^T\ \ \lambda_j\mathbf{\Phi}_j^T\}^T$ where $\mathbf{\Phi}_j$ indicates the *j*th complex mode shape of the combined building–TMD system. From the last row of Eq. (10)

$$\frac{k_s}{m_s}\psi_{l,j}-\frac{k_s}{m_s}\psi_{N,j}+\frac{c_s}{m_s}\psi_{N+l,j}-\frac{c_s}{m_s}\psi_{2N,j}-\lambda_j\psi_{2N,j}=0\,, \tag{13}$$

the damping ratio ξ_s of the TMD can be obtained and expressed in terms of the *j*th eigenparameter and natural frequency of the TMD, ω_s, as

$$\xi_s=\frac{\lambda_j\psi_{2N,j}-\omega_s^2(\psi_{l,j}-\psi_{N,j})}{2\omega_s(\psi_{N+l,j}-\psi_{2N,j})} \tag{14}$$

If the *j*th and *k*th eigenparameters are available, it can be written as

$$\frac{\lambda_j\psi_{2N,j}-\omega_s^2(\psi_{l,j}-\psi_{N,j})}{2\omega_s(\psi_{N+l,j}-\psi_{2N,j})}=\frac{\lambda_k\psi_{2N,k}-\omega_s^2(\psi_{l,k}-\psi_{N,k})}{2\omega_s(\psi_{N+l,k}-\psi_{2N,k})} \tag{15}$$

Therefore, the natural frequency of TMD is obtained as

$$\omega_s=\sqrt{\frac{\lambda_k\psi_{2N,k}(\psi_{N+l,j}-\psi_{2N,j})-\lambda_j\psi_{2N,j}(\psi_{N+l,k}-\psi_{2N,k})}{(\psi_{N+l,j}-\psi_{2N,j})(\psi_{l,k}-\psi_{N,k})-(\psi_{N+l,k}-\psi_{2N,k})(\psi_{l,j}-\psi_{N,j})}} \tag{16}$$

Eq. (16) shows that ω_s can be calculated from two sets of complex eigenparameters of the building–TMD system, which is identifiable from dynamic-response measurements by using state–space-based system-identification techniques. Once ω_s is obtained from Eq. (16), the damping ratio of TMD, ξ_s, can then be calculated using Eq. (14). To obtain ω_s and ξ_s, the eigenvalues and eigenvectors of the two complex modes (which are equivalent to one normal mode) are required, which indicates that only the eigenvector values at the two degrees of freedom, representing the TMD and *l*th floor at which the TMD is located, are required.

2.3 Identification of the primary building

2.3.1 Damping and stiffness coefficients of the lth story in which the TMD is located

To obtain the dynamic parameters of the primary building, the derivation begins at the *l*th row of Eq. (10) as follows

$$\begin{aligned}&\frac{k_{p_l}}{m_{p_l}}\psi_{l-1,j}-\frac{k_{p_l}}{m_{p_l}}\psi_{l,j}-\frac{k_{p_{l+1}}}{m_{p_l}}\psi_{l,j}-\frac{k_s}{m_{p_l}}\psi_{l,j}+\frac{k_{p_{l+1}}}{m_{p_l}}\psi_{l+1,j}+\frac{k_s}{m_{p_l}}\psi_{N,j}\\&+\frac{c_{p_l}}{m_{p_l}}\psi_{n+l,j}-\frac{c_{p_l}}{m_{p_l}}\psi_{N+l,j}-\frac{c_{p_{l+1}}}{m_{p_l}}\psi_{N+l,j}-\frac{c_s}{m_{p_l}}\psi_{N+l,j}-\lambda_j\psi_{N+l,j}+\frac{c_{p_{l+1}}}{m_{p_l}}\psi_{N+l+1,j}+\frac{c_s}{m_{p_l}}\psi_{2N,j}=0\end{aligned} \tag{17}$$

According to Eq. (17), the damping coefficient of the *l*th story of the primary building can be derived and expressed as

$$\begin{aligned}c_{p_l}=&c_{p_{l+1}}\frac{(\psi_{N+l,j}-\psi_{N+l+1,j})}{(\psi_{n+l,j}-\psi_{N+l,j})}+k_{p_{l+1}}\frac{(\psi_{l,j}-\psi_{l+1,j})}{(\psi_{n+l,j}-\psi_{N+l,j})}\\&+c_s\frac{(\psi_{N+l,j}-\psi_{2N,j})}{(\psi_{n+l,j}-\psi_{N+l,j})}+k_s\frac{(\psi_{l,j}-\psi_{N,j})}{(\psi_{n+l,j}-\psi_{N+l,j})}+\frac{\lambda_j\psi_{N+l,j}m_{p_l}}{(\psi_{n+l,j}-\psi_{N+l,j})}-k_{p_l}\frac{(\psi_{l-1,j}-\psi_{l,j})}{(\psi_{n+l,j}-\psi_{N+l,j})}\end{aligned} \tag{18}$$

Next, any two complex modes can be selected (e.g., *j*th and *k*th modes), and the stiffness coefficient of the *l*th story of the primary building can be derived on the basis of Eq. (18) as

$$\begin{aligned}k_{p_l}=&\left[\frac{(\psi_{l-1,k}-\psi_{l,k})}{(\psi_{n+l,k}-\psi_{N+l,k})}-\frac{(\psi_{l-1,j}-\psi_{l,j})}{(\psi_{n+l,j}-\psi_{N+l,j})}\right]^{-1}\\&\cdot\left[\frac{\hat{C}_{l+1,k}}{(\psi_{n+l,k}-\psi_{N+l,k})}-\frac{\hat{C}_{l+1,j}}{(\psi_{n+l,j}-\psi_{N+l,j})}+\frac{\hat{K}_{l+1,k}}{(\psi_{n+l,k}-\psi_{N+l,k})}-\frac{\hat{K}_{l+1,j}}{(\psi_{n+l,j}-\psi_{N+l,j})}\right.\\&+\frac{\hat{C}_{s_{l,k}}}{(\psi_{n+l,k}-\psi_{N+l,k})}-\frac{\hat{C}_{s_{l,j}}}{(\psi_{n+l,j}-\psi_{N+l,j})}+\frac{\hat{K}_{s_{l,k}}}{(\psi_{n+l,k}-\psi_{N+l,k})}-\frac{\hat{K}_{s_{l,j}}}{(\psi_{n+l,j}-\psi_{N+l,j})}\\&\left.+\frac{\lambda_k\psi_{N+l,k}m_{p_l}}{(\psi_{n+l,k}-\psi_{N+l,k})}-\frac{\lambda_j\psi_{N+l,j}m_{p_l}}{(\psi_{n+l,j}-\psi_{N+l,j})}\right]\end{aligned} \tag{19}$$

where $\hat{K}_{l+1,j}=k_{p_{l+1}}(\psi_{l,j}-\psi_{l+1,j})$, $\hat{C}_{l+1,j}=c_{p_{l+1}}(\psi_{N+l,j}-\psi_{N+l+1,j})$, $\hat{K}_{s_{l,j}}=k_s(\psi_{l,j}-\psi_{N,j})$, and $\hat{C}_{s_{l,j}}=c_s(\psi_{N+l,j}-\psi_{2N,j})$. In Eq. (19), parameters c_s and k_s can be solved from Eq. (14) and Eq. (16), respectively, which determine $\hat{C}_{s_{l,j}}$, $\hat{K}_{s_{l,j}}$, $\hat{C}_{s_{l,k}}$, and $\hat{K}_{s_{l,k}}$. In addition, the information related to the (l+1) story (i.e., $\hat{K}_{l+1,j}$, $\hat{K}_{l+1,k}$, $\hat{C}_{l+1,j}$, and $\hat{C}_{l+1,k}$) can be solved in advance (as shown in the next section). The floor masses of the primary building and TMD are assumed to be known, and Eqs. (18) and (19) are then solved sequentially. In addition, Eqs. (18) and (19) are applied to calculate the stiffness and damping coefficients of the other inner story, at which the TMD is not installed, by setting $\hat{C}_{s_{l,j}}$, $\hat{K}_{s_{l,j}}$, $\hat{C}_{s_{l,k}}$, and $\hat{K}_{s_{l,k}}$ to 0.

2.3.2 Damping and stiffness coefficients of the top story

For the top story, Eq. (19) can be applied by setting $\hat{K}_{l+1,j}=\hat{K}_{l+1,k}=\hat{C}_{l+1,j}=\hat{C}_{l+1,k}=0$. In addition, assigning $l=n$ in Eq. (19) leads to

$$k_{p_n}=\left[\frac{(\psi_{n-1,k}-\psi_{n,k})}{(\psi_{2n,k}-\psi_{2N-1,k})}-\frac{(\psi_{n-1,j}-\psi_{n,j})}{(\psi_{2n,j}-\psi_{2N-1,j})}\right]^{-1}\cdot\left[\frac{\lambda_k\psi_{2N-1,k}m_{p_n}}{(\psi_{2n,k}-\psi_{2N-1,k})}-\frac{\lambda_j\psi_{2N-1,j}m_{p_n}}{(\psi_{2n,j}-\psi_{2N-1,j})}+\frac{\hat{C}_{s_{n,k}}}{(\psi_{2n,k}-\psi_{2N-1,k})}-\frac{\hat{C}_{s_{n,j}}}{(\psi_{2n,j}-\psi_{2N-1,j})}+\frac{\hat{K}_{s_{n,k}}}{(\psi_{2n,k}-\psi_{2N-1,k})}-\frac{\hat{K}_{s_{n,j}}}{(\psi_{2n,j}-\psi_{2N-1,j})}\right] \tag{20a}$$

Furthermore, setting $c_{p_{l+1}}=k_{p_{l+1}}=0$ and $l=n$ in Eq. (18) gives

$$c_{p_n}=c_s\frac{(\psi_{N+n,j}-\psi_{2N,j})}{(\psi_{2n,j}-\psi_{N+n,j})}+k_s\frac{(\psi_{n,j}-\psi_{N,j})}{(\psi_{2n,j}-\psi_{N+n,j})}+\frac{\lambda_j\psi_{N+n,j}m_{p_n}}{(\psi_{2n,j}-\psi_{N+n,j})}-k_{p_n}\frac{(\psi_{n-1,j}-\psi_{n,j})}{(\psi_{2n,j}-\psi_{N+n,j})} \tag{20b}$$

In a situation in which the TMD is not installed at the nth floor, then c_s, k_s, $\hat{C}_{s_{n,j}}$, $\hat{K}_{s_{n,j}}$, $\hat{C}_{s_{n,k}}$, and $\hat{K}_{s_{n,k}}$ are all equal to zero.

2.3.3 Damping and stiffness coefficients of the first story

For the first story (i.e., when $l=1$), $\psi_{l-1,j}$, $\psi_{l-1,k}$, $\psi_{n+l,j}$, and $\psi_{n+l,k}$ are eliminated and are all equal to 0 in Eqs. (18) and (19). The following equations can be derived

$$k_{p_1}=\left(\frac{\psi_{1,k}}{\psi_{N+1,k}}-\frac{\psi_{1,j}}{\psi_{N+1,j}}\right)^{-1}\cdot\left(-\frac{\hat{C}_{1+1,k}}{\psi_{N+1,k}}+\frac{\hat{C}_{1+1,j}}{\psi_{N+1,j}}-\frac{\hat{K}_{1+1,k}}{\psi_{N+1,k}}+\frac{\hat{K}_{1+1,j}}{\psi_{N+1,j}}-\frac{\hat{C}_{s_{1,k}}}{\psi_{N+1,k}}+\frac{\hat{C}_{s_{1,j}}}{\psi_{N+1,j}}-\frac{\hat{K}_{s_{1,k}}}{\psi_{N+1,k}}+\frac{\hat{K}_{s_{1,j}}}{\psi_{N+1,j}}-\lambda_k m_{p_1}+\lambda_j m_{p_1}\right) \tag{21a}$$

$$c_{p_1}=c_{p_2}\frac{\psi_{N+2,j}-\psi_{N+1,j}}{\psi_{N+l,j}}+k_{p_2}\frac{\psi_{2,j}-\psi_{1,j}}{\psi_{N+l,j}}+c_s\frac{\psi_{2N,j}-\psi_{N+1,j}}{\psi_{N+1,j}}+k_s\frac{\psi_{N,j}-\psi_{1,j}}{\psi_{N+1,j}}-\frac{\lambda_j\psi_{N+1,j}m_{p_1}}{\psi_{N+1,j}}-k_{p_1}\frac{\psi_{1,j}}{\psi_{N+1,j}} \tag{21b}$$

Table 1 Physical parameters of two 3-story buildings in the numerical study

Physical Parameters	CASE-1: Ideal shear building	CASE-2: Real benchmark building
Mass matrix (kg)	$\begin{bmatrix} 6000 & 0 & 0 \\ 0 & 6000 & 0 \\ 0 & 0 & 6000 \end{bmatrix}$	$\begin{bmatrix} 6000 & 0 & 0 \\ 0 & 6000 & 0 \\ 0 & 0 & 6000 \end{bmatrix}$ 1F 2F 3F
Damping matrix (*kN*-sec/m)	$\begin{bmatrix} 13.6 & -7.90 & 0 \\ -7.90 & 13.3 & -5.40 \\ 0 & -5.40 & 5.40 \end{bmatrix}$	$\begin{bmatrix} 13.28 & -8.701 & 1.463 \\ -8.701 & 13.557 & -5.774 \\ 1.463 & -5.774 & 5.657 \end{bmatrix}$ 1F 2F 3F
Stiffness Matrix (kN/m)	$\begin{bmatrix} 3300 & -1600 & 0 \\ -1600 & 3100 & -1500 \\ 0 & -1500 & 1500 \end{bmatrix}$	$\begin{bmatrix} 3406 & -1814 & 138.2 \\ -1814 & 3329 & -1672 \\ 138.2 & -1672 & 1509 \end{bmatrix}$ 1F 2F 3F

Table 2 Real modal parameters of two 3-story buildings in the numerical study

Modal Parameters	CASE-1: Ideal shear building	CASE-2: Real benchmark building
Frequency, $\{\omega_{0_1} \ \omega_{0_2} \ \omega_{0_3}\}$ (Hz)	$\{1.17 \ 3.22 \ 4.65\}$	$\{1.04 \ 3.17 \ 4.86\}$
Damping ratio, $\{\xi_{0_1} \ \xi_{0_2} \ \xi_{0_3}\}$ (%)	$\{1.45 \ 3.65 \ 6.32\}$	$\{1.99 \ 3.07 \ 6.43\}$
Mode shape, $\{\boldsymbol{\varphi}_{0_1} \ \boldsymbol{\varphi}_{0_2} \ \boldsymbol{\varphi}_{0_3}\}$	$\begin{bmatrix} 0.421 & -1.194 & 2.124 \\ 0.783 & -0.634 & -2.420 \\ 1.000 & 1.000 & 1.000 \end{bmatrix}$	$\begin{bmatrix} 0.408 & -1.247 & 1.954 \\ 0.784 & -0.627 & -2.291 \\ 1.000 & 1.000 & 1.000 \end{bmatrix}$ 1F 2F 3F

Table 3 Parameters of the TMD for two 3-story buildings in the numerical study

TMD Parameters	CASE-1	CASE-2
Mass ratio, μ (Mass, m_s)	2% (360 kg)	
Damping ratio, $(\xi_s)_{opt}$	7.03%	
Frequency ratio, $(r_f)_{opt}$	0.965	
Natural frequency, ω_s	1.129 Hz	1.001 Hz
Damping coefficient, c_s (*k*N-sec/m)	0.361	0.318
Stiffness coefficient, k_s (*k*N/m)	18.242	14.226

In a situation in which the TMD is not installed at the first floor, then $\hat{C}_{s_{1,j}} = \hat{K}_{s_{1,j}} = \hat{C}_{s_{1,k}} = \hat{K}_{s_{1,k}} = 0$ is assigned.

3. Numerical verifications

To verify the accuracy of the aforementioned methodology, numerical studies for two three-story buildings were conducted. The primary structure of the first case (CASE-1) is a

shear-type building, whereas the structure of the second case (CASE-2) is a real benchmark building, for which the damping and stiffness matrices are full matrices. The physical and normal-mode modal parameters of these two buildings are presented in Tables 1 and 2. The accuracy of the proposed parameter-extraction procedure was investigated using different building types to examine its applicability to evaluating TMD performance in real building–TMD structures.

3.1 TMD design parameters

A TMD with a mass of 360 kg, 2% of the total mass of the three-story building, was assumed. The optimal frequency ratio and damping ratio of the TMD can be obtained on the basis of the design formulas proposed by Lin *et al.* (1994), as follows

$$(r_f)_{opt} = \left(\frac{a}{1+\mu}\right)^b; \quad a = 1.0 - \frac{\xi_p}{4}, \quad b = 1.35e^{3.2\xi_p} \tag{22}$$

$$(\xi_s)_{opt} = 0.46\mu^{0.48} \tag{23}$$

where μ represents the ratio of the mass of the TMD to the total mass of the building and ξ_p denotes the damping ratio of the controlled mode of the building. The TMD was assumed to be installed on the roof (third floor) of the building. The system parameters of the TMD for controlling the first mode of the building were calculated using Eqs. (22) and (23) (Table 3) and were then used to generate the mass, damping, and stiffness matrices of the building–TMD system.

3.2 Identification procedure

The following analysis procedure is used for extracting the dynamic properties of the TMD and building structure:

Step 1:

The time traces of the acceleration response of each floor and TMD are generated using step-by-step numerical methods. For the input–output situation, the ground acceleration recorded at National Chung Hsing University (NCHU) in the east–west direction during the 1999 Taiwan Chi-Chi earthquake was used as the base excitation; for the output-only situation, the building–TMD system response was excited using a base excitation of normally-distributed white noise with a zero mean and a standard deviation (STD) of 0.5 gal.

Step 2:

The System Realization Using Information Matrix (SRIM) identification technique (Juang 1997, Lin *et al*. 2005, Lin *et al*. 2008, Lin *et al*. 2010) is employed based on the selected system input and output measurements for the input–output situation in Step 1. Regarding the output-only situation, the stochastic subspace identification (SSI) (Van Overschee and De Moor 2011) method is employed on the basis of the output response of the building–TMD system. Transforming discrete time into continuous time may obtain the optimal realization of the state–space system matrix $\mathbf{A}$.

Step 3:

The continuous-time eigenvalue λ_j and eigenvector $\mathbf{\Psi}_j$ of system matrix $\mathbf{A}$ are computed (where j = 1–8);

Step 4:

With the known system parameters $\mathbf{M}_p$, m_s, λ_j, and $\mathbf{\Psi}_j$ (where j = 1–8), the TMD's modal parameters ω_s and ξ_s are computed using Eqs. (16) and (14), respectively, and k_{p_n}, c_{p_n}, $k_{p_{n-1}}$, $c_{p_{n-1}}$, …, k_{p_1}, and c_{p_1} are then computed sequentially by using Eqs. (18)-(21). In the following sections, the notations of $\hat{\omega}_s$, $\hat{\xi}_s$, $\hat{k}_{p_n}$, $\hat{c}_{p_n}$, $\hat{k}_{p_{n-1}}$, $\hat{c}_{p_{n-1}}$, …, $\hat{k}_{p_1}$, and $\hat{c}_{p_1}$ are used to represent the identified parameters to distinguish between the real and reference values.

3.3 Results and discussion

3.3.1 Input–output situation: Full measurements

Because the building–TMD system has four degrees of freedom (n = 3 and N = 4), eight sets of eigenparameters were obtained using Steps 1 to 3. The eight eigenvalues and four corresponding real modal frequencies and damping ratios are as follows

CASE-1:

$$\begin{Bmatrix}\lambda_1,\lambda_2\\ \lambda_3,\lambda_4\\ \lambda_5,\lambda_6\\ \lambda_7,\lambda_8\end{Bmatrix}=\begin{Bmatrix}-0.276\pm 6.62i\\ -0.345\pm 7.88i\\ -0.751\pm 20.2i\\ -1.850\pm 29.2i\end{Bmatrix},\quad \begin{Bmatrix}\omega_1\\ \omega_2\\ \omega_3\\ \omega_4\end{Bmatrix}=\begin{Bmatrix}1.06\\ 1.26\\ 3.22\\ 4.65\end{Bmatrix}\text{(Hz)},\quad \begin{Bmatrix}\xi_1\\ \xi_2\\ \xi_3\\ \xi_4\end{Bmatrix}=\begin{Bmatrix}4.17\\ 4.37\\ 3.71\\ 6.33\end{Bmatrix}\text{(\%)} \tag{24a}$$

CASE-2:

$$\begin{Bmatrix}\lambda_1,\lambda_2\\ \lambda_3,\lambda_4\\ \lambda_5,\lambda_6\\ \lambda_7,\lambda_8\end{Bmatrix}=\begin{Bmatrix}-0.259\pm 5.85i\\ -0.326\pm 6.98i\\ -0.623\pm 19.9i\\ -1.970\pm 30.5i\end{Bmatrix},\quad \begin{Bmatrix}\omega_1\\ \omega_2\\ \omega_3\\ \omega_4\end{Bmatrix}=\begin{Bmatrix}0.93\\ 1.11\\ 3.18\\ 4.87\end{Bmatrix}\text{(Hz)},\quad \begin{Bmatrix}\xi_1\\ \xi_2\\ \xi_3\\ \xi_4\end{Bmatrix}=\begin{Bmatrix}4.42\\ 4.67\\ 3.12\\ 6.44\end{Bmatrix}\text{(\%)} \tag{24b}$$

Obviously, the first mode of the primary building (ω_{0_1} in Table 2) is split into lower- and higher-frequency modes (ω_1 and ω_2), showing that the TMD is tuned to the first mode of the primary building. Both the first and second modal damping ratios (ξ_1 and ξ_2) are larger than that of the original first mode (ξ_{0_1} in Table 2), indicating that the TMD increases the energy dissipation capability of the primary building. However, if the modal properties of the primary building (ω_{0_1} and ξ_{0_1}) are unknown, it is difficult to determine the difference between buildings with and without the TMD, as well as the efficacy of the TMD.

The first, third, fifth, and seventh eigenvectors are as follows

CASE-1:

$$\begin{aligned}&\{\mathbf{\Psi}_1\ \mathbf{\Psi}_3\ \mathbf{\Psi}_5\ \mathbf{\Psi}_7\}\\ &=\begin{bmatrix}-0.0126+0.00003i & 0.0171+0.01455i & 0.0948+0.13342i & -0.0937-0.12115i\\ -0.0239-0.00018i & 0.0309+0.02704i & 0.0506+0.06973i & 0.1059+0.13887i\\ -0.0317-0.00052i & 0.0376+0.03394i & -0.0815-0.11117i & -0.0424-0.05886i\\ -0.2121-0.06771i & -0.2018-0.07846i & 0.0173+0.01136i & 0.0045+0.00249i\\ 0.0037+0.08330i & 0.1088-0.13953i & 2.6276-2.01770i & -3.3606+2.95710i\\ 0.0054+0.15816i & 0.2025-0.25255i & 1.3724-1.07630i & 3.8547-3.34680i\\ 0.0053+0.21026i & 0.2545-0.30836i & -2.1874+1.73210i & -1.6386+1.34510i\\ -0.3899+1.4237i & -0.5487+1.6178i & 0.2167-0.35850i & 0.0643-0.13582i\end{bmatrix}\end{aligned} \tag{25a}$$

CASE-2:

$$\{\boldsymbol{\Psi}_1\ \boldsymbol{\Psi}_3\ \boldsymbol{\Psi}_5\ \boldsymbol{\Psi}_7\} = \begin{bmatrix} -0.0121+0.00004i & 0.0176+0.01305i & 0.1059+0.12878i & -0.1081-0.10478i \\ -0.0238-0.00007i & 0.0331+0.02506i & 0.0532+0.06405i & 0.1259+0.12396i \\ -0.0313-0.00031i & 0.0408+0.03166i & -0.0866-0.10252i & -0.0545-0.05491i \\ -0.2142-0.06053i & -0.2043-0.07046i & 0.0143+0.00717i & 0.0039+0.00109i \\ 0.0034+0.07087i & 0.0853-0.12676i & 2.5027-2.19270i & -2.9835+3.5051i \\ 0.0057+0.13901i & 0.1640-0.23883i & 1.2444-1.10060i & 3.5334-4.0837i \\ 0.0063+0.18290i & 0.2076-0.29490i & -1.9910+1.79210i & -1.5677+1.7702i \\ -0.2987+1.26870i & -0.4251+1.44830i & 0.1340-0.29007i & 0.0255-0.12013i \end{bmatrix} \quad (25b)$$

Besides, $\{\boldsymbol{\Psi}_2\ \boldsymbol{\Psi}_4\ \boldsymbol{\Psi}_6\ \boldsymbol{\Psi}_8\} = \{\overline{\boldsymbol{\Psi}}_1\ \overline{\boldsymbol{\Psi}}_3\ \overline{\boldsymbol{\Psi}}_5\ \overline{\boldsymbol{\Psi}}_7\}$; the "bar" notation denotes a conjugate computation.

Table 4 presents the obtained parameters of the TMD and primary building by using the proposed method. As shown in Table 4, $\{\hat{\omega}_{0_1}, \hat{\omega}_{0_2}, \hat{\omega}_{0_3}\}$ and $\{\hat{\xi}_{0_1}, \hat{\xi}_{0_2}, \hat{\xi}_{0_3}\}$ were the identified real modal frequencies and damping ratios of the reconstructed shear building based on $\{\hat{c}_{p_1}, \hat{c}_{p_2}, \hat{c}_{p_3}\}$ and $\{\hat{k}_{p_1}, \hat{k}_{p_2}, \hat{k}_{p_3}\}$. In theory, the proposed method can be implemented by selecting any two sets of eigenvalues and eigenvectors, namely (λ_j, $\boldsymbol{\Psi}_j$) and (λ_k, $\boldsymbol{\Psi}_k$). The results of CASE-1 showed that the identified parameters of the TMD and primary building were the same as the original parameters (Tables 2 and 3), regardless of the selection of (*j*, *k*) set. For CASE-2, the TMD parameters were also accurately identified regardless of the selection of (*j*, *k*) set. The results showed that the identified "pseudoshear" building was related to the selection of (*j*, *k*); it was difficult to assess which set of the identified physical parameters could optimally represent the CASE-2 building. However, although the modal parameters of the reconstructed shear building could not fully represent the original building, selecting the (*j*, *k*) pairs resulted in the optimal estimation of the corresponding building mode. Specifically, selecting (*j*, *k*) = (1, 2) or (3, 4) resulted in the optimal $\hat{\omega}_{0_1}$ and $\hat{\xi}_{0_1}$, selecting (*j*, *k*) = (5, 6) resulted in the optimal $\hat{\omega}_{0_2}$ and $\hat{\xi}_{0_2}$, and continued in a trend of optimally selected pairs and resulting estimations. These results indicate that it is always possible to obtain modal parameters of a building that are more accurate by selecting various (*j*, *k*) pairs.

3.3.2 Input–output situation: Partial measurements

In practice, building floors are not fully measured because of a limited number of sensors. To apply the proposed method to partial-measurement situations, the primary building was regarded as an equivalent shear building with a floor number equal to the number of measured floors (denoted as *m*). The total mass of the building was redistributed and grouped as the *m*-measured floors, and the physical parameters of the reduced shear building were identified. The modal frequency and modal damping ratio of the equivalent building were then calculated.

For illustrative purposes, available outputs can be assumed for the measurements of the mass of the TMD and third floor in which the TMD is located for the CASE-1 and CASE-2 buildings. The steps in Section 3.2 were used to calculate the parameters of the TMD and equivalent single-story shear building of both cases (Table 5). The results showed that the identified TMD parameters were still accurate in these two single-measurement cases.

Table 4 Identified parameters of the TMD and primary buildings in the numerical study (full measurement)

Identified Parameters		(*j*, *k*)	CASE-1	CASE-2
TMD	$\hat{\omega}_s$ (Hz)	(1, 2), (3,4), (5,6),	1.13	1.00
	$\hat{\xi}_s$ (%)	or (7,8)	7.03	7.03
Primary building (physical)	$\{\hat{c}_{p_1}, \hat{c}_{p_2}, \hat{c}_{p_3}\}$ (*k*N-sec/m)	(1, 2)	{5.7, 7.9, 5.4}	{7.801, 7.523, 5.512}
		(3, 4)		{7.637, 7.488, 3.913}
		(5, 6)		{4.922, 5.374, 4.333}
		(7, 8)		{7.170, 7.830, 6.255}
	$\{\hat{k}_{p_1}, \hat{k}_{p_2}, \hat{k}_{p_3}\}$ (*k*N/m)	(1, 2)	{1700, 1600, 1500}	{1330, 1170, 1166}
		(3, 4)		{1336, 1164, 1155}
		(5, 6)		{1784, 1209, 1379}
		(7, 8)		{1733, 1782, 1604}
Primary building (modal)	$\{\hat{\omega}_{0_1}, \hat{\omega}_{0_2}, \hat{\omega}_{0_3}\}$ (Hz)	(1, 2)	{1.17, 3.22, 4.65}	{**1.04**, 2.86, 4.05}
		(3, 4)		{**1.03**, 2.78, 3.98}
		(5, 6)		{1.13, **3.17**, 4.29}
		(7, 8)		{1.22, 3.34, **4.86**}
	$\{\hat{\xi}_{0_1}, \hat{\xi}_{0_2}, \hat{\xi}_{0_3}\}$ (%)	(1, 2)	{1.45, 3.65, 6.32}	{**1.94**, 4.75, 7.35}
		(3, 4)		{**1.86**, 3.99, 6.95}
		(5, 6)		{1.27, **3.07**, 5.01}
		(7, 8)		{1.61, 4.22, **6.43**}

Table 5 Identified parameters of the TMD and primary buildings in the numerical study (single-floor measurement)

Identified Parameters		(*j*, *k*)	CASE-1	CASE-2
TMD	$\hat{\omega}_s$ (Hz)	(1, 2), (3,4), (5,6),	1.13	1.00
	$\hat{\xi}_s$ (%)	or (7,8)	7.03	7.03
Primary building (physical)	$\hat{c}_p$ (*k*N-sec/m)	(1, 2)	6.459	6.661
		(3, 4)	7.134	7.427
		(5, 6)	26.59	22.02
		(7, 8)	66.19	70.56
	$\hat{k}_p$ (*k*N/m)	(1, 2)	898.64	703.05
		(3, 4)	1032.1	809.70
		(5, 6)	7354.3	7152.7
		(7, 8)	15358	16805
Primary building (modal)	$\hat{\omega}_0$ (Hz)	(1, 2)	1.12	0.99
		(3, 4)	1.21	1.07
		(5, 6)	3.22	3.17
		(7, 8)	4.65	4.86
	$\hat{\xi}_0$ (%)	(1, 2)	2.54	2.96
		(3, 4)	2.62	3.08
		(5, 6)	3.65	3.07
		(7, 8)	6.29	6.41

Regarding the primary building, the identified $\hat{\omega}_0$ and $\hat{\xi}_0$ values were highly dependent on the selected mode pair (j, k). When (j, k) = (1, 2) or (3, 4), which is related to the first mode, $\hat{\omega}_0$ and $\hat{\xi}_0$ were close to ω_{0_1} (1.17 Hz in CASE-1 and 1.04 Hz in CASE-2) and ξ_{0_1} (1.45% in CASE-1 and 1.99% in CASE-2), respectively. However, the situation of (j, k) = (3, 4) led to smaller errors. When (j, k) = (5, 6), $\hat{\omega}_0$ and $\hat{\xi}_0$ were close to ω_{0_2} and ξ_{0_2}, respectively, with the trend continuing similarly. The percentage errors of the identified parameters were also calculated using the true values of the corresponding building modes. Specifically, when (j, k) = (1, 2) or (3, 4), the percentage error of $\hat{\omega}_0$ was defined as $(\hat{\omega}_0 - \omega_{0_1})/\omega_{0_1}$. The analysis results showed that the errors of identified second and third modes (which were the uncontrolled modes) were smaller than those of the first mode. The absolute error in the first modal frequency was less than 5% and could be reduced by averaging the results of (j, k) = (1, 2) and (j, k) = (3, 4). In addition, the identified first modal damping ratios were overestimated but acceptable because the damping ratio was always the most difficult parameter to identify accurately.

3.3.3 Output–only situation

Typically, the dynamic responses of tall buildings are frequently excited by environmental loadings (rather than by an earthquake) in which the input sources are uncertain and unmeasurable.

In this situation, the output-only system identification method is a suitable solution for evaluating the dynamic parameters of structures. To simulate such a circumstance, the output acceleration responses of the floors and TMD of the CASE-2 system subjected to a white-noise input (STD = 0.5 gal) were obtained, and the SSI method was employed to identify the complex eigenvalues and eigenvectors of the combined system. These eigenparameters were then used to extract the respective dynamic parameters of the primary building and TMD.

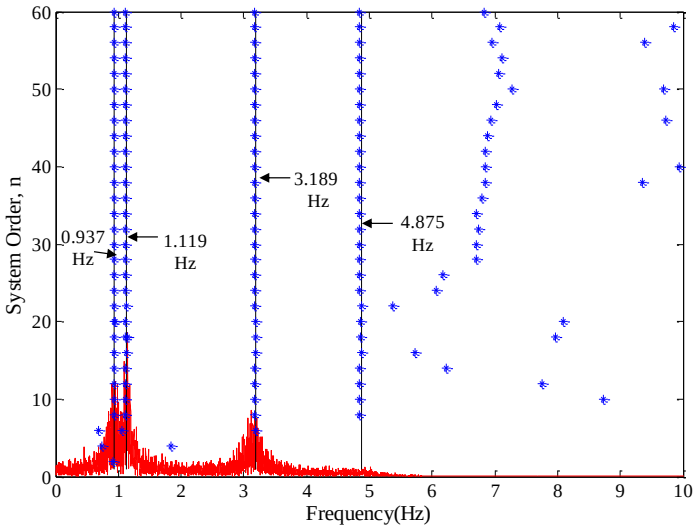

Fig. 2 Stabilization diagram of the identified modal frequencies of the CASE-2 building–TMD system produced using the SSI method (asterisks mark the modal frequencies; the background curve is the Fourier amplitude of the roof acceleration response)

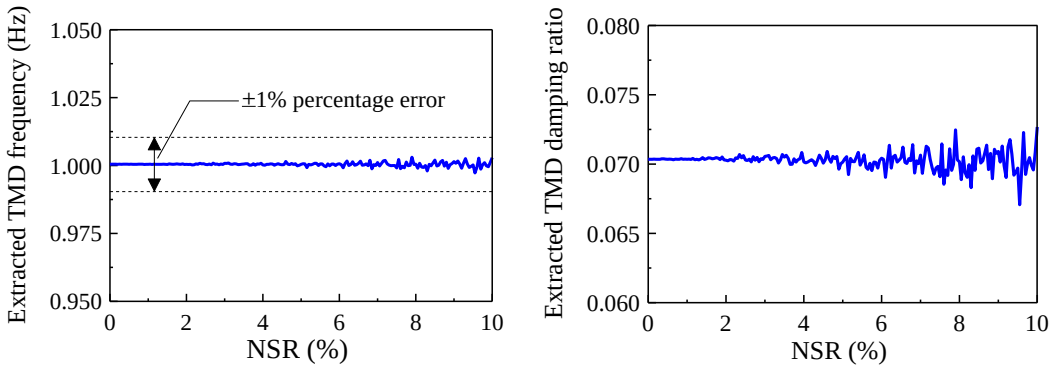

Fig. 3 Extracted frequency and damping ratio of the TMD at various noise scales determined using the SSI method (CASE-2 system)

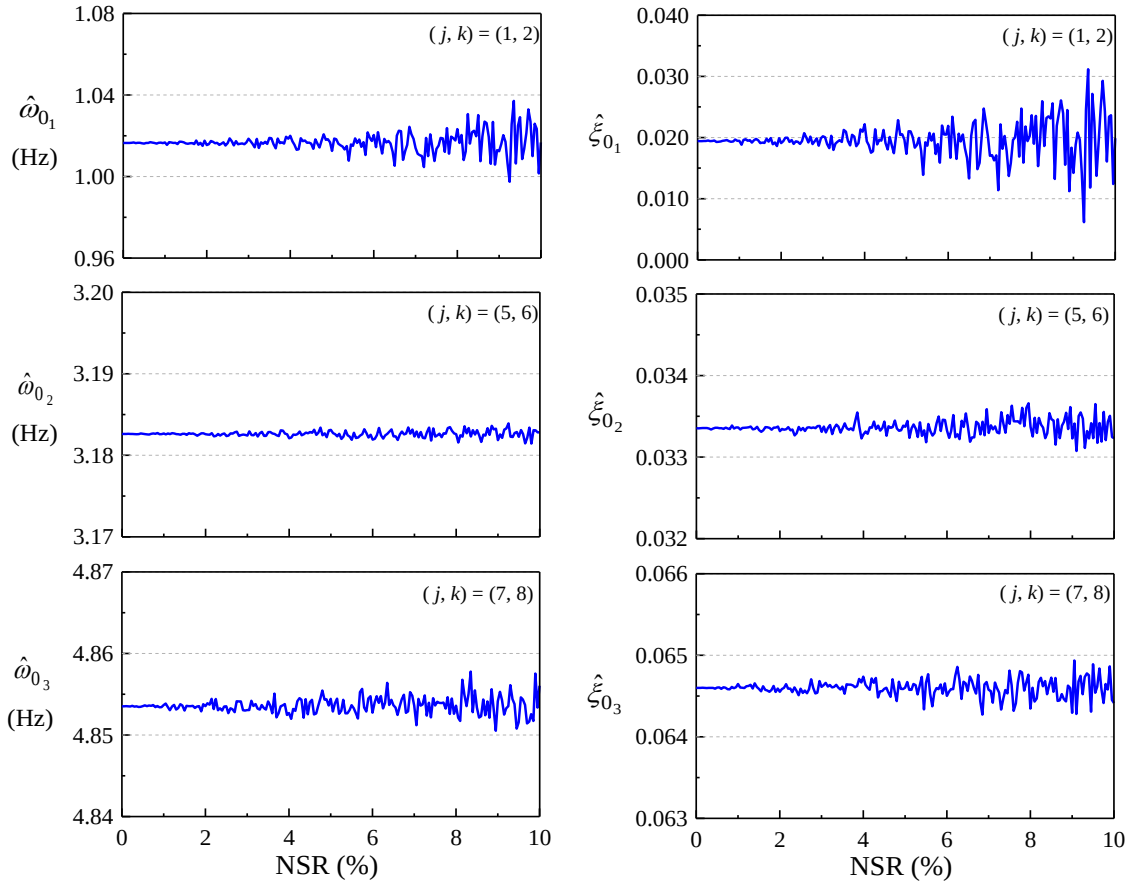

Fig. 4 Extracted modal frequencies and damping ratios of the primary building at various noise scales determined using the SSI method (CASE-2 system)

In this output-only situation, an additional white noise was added to each output response to simulate the unavailable noise contaminated in measured signals. The NSR is defined as the ratio of the noise STD to the input STD. Typically, the noise STD of a high-precision sensor is smaller than 0.05 gal. First, to determine the system order when employing the SSI method, the stabilization diagram of the building–TMD system without noise was established (Fig. 2). Four stable frequencies were detected when the system order n $\geqq$ 8. The first two frequencies (0.937 Hz and 1.119 Hz) were clearly split from the first modal frequency (1.04Hz) of the primary building because of the existence of the TMD, whereas the third and fourth frequencies (3.189 Hz and 4.875 Hz) were close to the second and third modal frequencies of the primary building (3.17 Hz and 4.86 Hz) (Table 2). Based on these readings, the system order n = 8 was chosen for applying the SSI method at various NSR levels.

The eigenvalues and eigenvectors of the building–TMD system at different levels of NSR were identified, and the parameters of the TMD and primary building were extracted (Figs. 3 and 4). As shown in Fig. 3, the results indicated that the noise had little effect on the extracted parameters, particularly on the frequency of the TMD. This result was critical because the vibration-control effectiveness of the TMD is sensitive to the TMD frequency. As shown in the left column of Fig. 4, the extracted modal frequencies of the primary building varied within limited and acceptable ranges. The first modal damping ratio varied by approximately ±1%, which was an expected sensitivity parameter. However, this variation had an insignificant effect on the TMD design parameters, according to Eqs. (22) and (23).

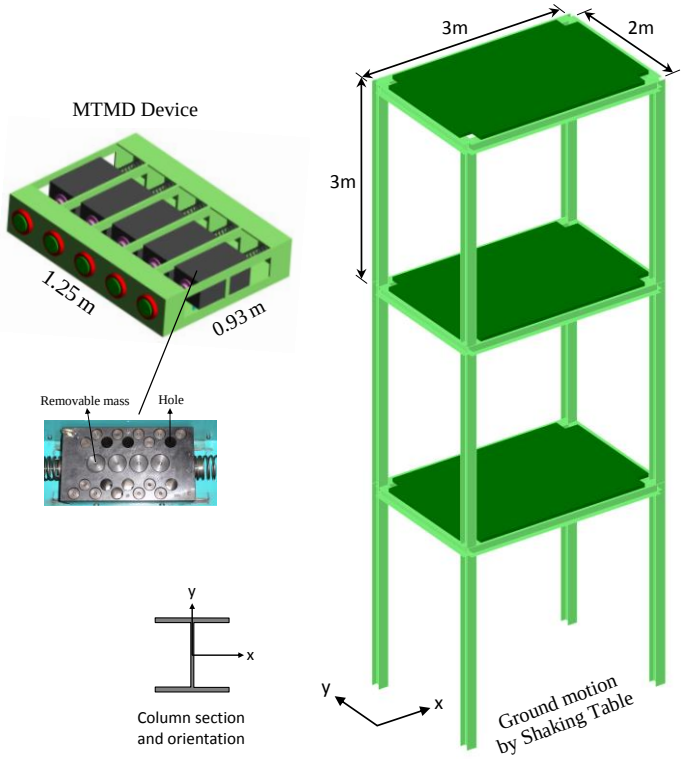

Fig. 5 Configuration of the experimental three-story building and MTMD device (Lin *et al.* 2010)

4. Experimental verification

The experimental data of the shaking-table tests were used to validate the proposed method. This experiment involved a large-scale, three-story steel frame equipped with multiple TMDs, and was conducted at the National Center for Research on Earthquake Engineering in Taiwan. This three-story structure was designed as a benchmark building for researching structural control and health monitoring. The building was uniform, weighing 18 t and measuring 9 m high. The dimension of the rectangular floor was 3 × 2 m. Each floor was constructed using a composite frame-plate structure and supplementary lead blocks and was supported by four columns with H-shape section (H 150 × 150 × 7 × 10). The orientation of the column section was arranged so that the weak direction of the building was parallel to the long side of the floor, which was also the moving direction of the shaking table. The details of the experimental layout and the shaking-table test of the three-story building were reported by Lin *et al.* (2010). Table 6 presents the identified modal parameters of the experimental building. They were similar to those of the CASE-2 building used in the numerical study, except that the second and third modal damping ratios of the experimental building were much smaller. The configuration of the building is shown in Fig. 5.

Table 6 Modal parameters of the experimental three-story building

Modal Parameters	Identified results
Frequency (Hz) $\{\omega_{0_1} \ \omega_{0_2} \ \omega_{0_3}\}$	$\{1.08 \ 3.24 \ 5.03\}$
Damping ratio (%) $\{\xi_{0_1} \ \xi_{0_2} \ \xi_{0_3}\}$	$\{2.19 \ 0.20 \ 0.16\}$
Mode shape $\{\boldsymbol{\varphi}_{0_1} \ \boldsymbol{\varphi}_{0_2} \ \boldsymbol{\varphi}_{0_3}\}$	$\begin{bmatrix} 0.401 & -1.156 & 1.742 \\ 0.736 & -0.504 & -1.879 \\ 1.000 & 1.000 & 1.000 \end{bmatrix}$ 1F 2F 3F

Table 7 Designed parameters of MTMD units

Parameters		Unit 1	Unit 2	Unit 3	Unit 4	Unit 5	Equivalent TMD
Mass (kg)		76	77	73	75	70	371
Optimal	ω_s, Hz	1.041	1.041	1.041	1.041	1.041	1.041
	(r_f)	(0.964)	(0.964)	(0.964)	(0.964)	(0.964)	(0.964)
	ξ_s, %	7.14	7.14	7.14	7.14	7.14	7.14
Assembled	ω_s, Hz	1.015	1.004	1.037	1.026	1.058	1.028
	(r_f)	(0.94)	(0.93)	(0.96)	(0.95)	(0.98)	(0.952)
	ξ_s, %	7.15	7.05	7.43	7.23	7.75	7.41

The MTMD setup was used to simulate a single TMD with mass of 371 kg, optimal damping coefficient of 346.4 N·s / m ($(\xi_s)_{opt} = 7.14\%$), and optimal stiffness coefficient of 15886 N/m ($(r_f)_{opt} = 0.964$))

4.1 Description of the TMD

The experiment was originally designed to verify the performance of a novel MTMD. An MTMD with five parallel units was assembled. Each unit consisted of a steel block, a coil spring, and an "airpot" damper device (Fig. 5). The spring of each unit was identical to those of the other units ($k_s = 3{,}099$ N/m), whereas the mass and damping of each unit were adjustable to achieve optimal unit frequencies and damping ratios. In one part of the experiment, the five units were adjusted to function similar to a single TMD. Table 7 shows the designed parameters and actual parameters of the five assembled MTMD units. Theoretically, each unit should have the same mass. However, it could not be achieved because the mass of the blocks exhibited limited adjustability. The assembled c_s and k_s values of each unit (Table 7) were based on the manufacturers' specifications. The parameters of the assembled TMD were close to those of the optimal TMD. In this experiment, the mass and damping of each MTMD unit were adjusted when the device was installed on the third floor of the benchmark building. The free-vibration tests of each unit with a fixed base could not be performed.

4.2 Identification of the building–TMD system

The building–MTMD system was excited using three base accelerations in sequence (i.e., NCHU campus record of the 1999 Taiwan Chi-Chi earthquake, white noise, and the 1940 El Centro earthquake). Because the allowable stroke of the MTMD unit was only 65 mm, the peak ground acceleration of each earthquake input was downscaled. During the test, the absolute accelerations and relative displacements of the five MTMD units were all measured. Fig. 6 illustrates the time histories and Fourier amplitudes of the displacement measurements of the five MTMD units. The results showed no obvious discrepancy between the motions of the five MTMD units, which indicates that the behavior of the MTMD was similar to that of a single TMD.

First, to identify the parameters of the entire building–TMD system, the SRIM identification technique was employed. The acceleration-time history at the base was set as the system input, and those at the three floors and TMD were set as the outputs. The average acceleration-time history of the five MTMD units was used to represent the TMD's motion. Next, the eigenvalues and eigenvectors of the eight complex modes of the combined building–TMD system were identified.

Table 8 Identified modal parameters of the building–TMD system

Modal Parameters	Identified results
Frequency (Hz) $\{\omega_1 \quad \omega_2 \quad \omega_3 \quad \omega_4\}$	$\{0.91 \;\; 1.13 \;\; 3.22 \;\; 5.02\}$
Damping ratio (%) $\{\xi_1 \quad \xi_2 \quad \xi_3 \quad \xi_4\}$	$\{6.27 \;\; 4.12 \;\; 0.29 \;\; 0.18\}$
Mode shape $\{\boldsymbol{\varphi}_1 \quad \boldsymbol{\varphi}_2 \quad \boldsymbol{\varphi}_3 \quad \boldsymbol{\varphi}_4\}$	$\begin{bmatrix} 0.363 & 0.412 & -1.181 & 1.867 \\ 0.693 & 0.748 & -0.540 & -1.993 \\ 1.000 & 1.000 & 1.000 & 1.000 \\ 9.363 & -3.445 & -0.166 & -0.108 \end{bmatrix}$ 1F 2F 3F TMD

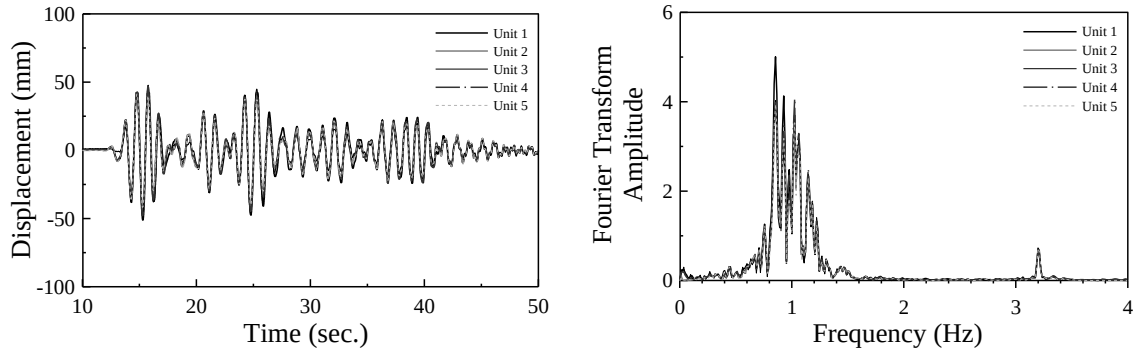

Fig. 6 Measured displacements and Fourier transform amplitudes of five MTMD units relative to the third floor under the downscaled ground motion of the Chi-Chi earthquake

The corresponding real modal parameters of the Chi-Chi earthquake situation are shown in Table 8. Results show that the identified third and fourth modes of the building–TMD system were close to the second and third modes of the primary building, respectively, whereas the first mode of the primary building (1.08 Hz) was split into two separate modes (0.91 and 1.13 Hz). In addition, the mode-shape value of the TMD was large at the first and second modes but small at the third and fourth modes, which indicates that the TMD was tuned to the first mode of the primary building. The damping ratios of the first two modes (6.27% and 4.12%) were larger than the first modal damping of the primary building (1.95%) and show the control effectiveness of the TMD, which dissipated more energy in the building.

4.3 Parameter extractions of TMD and primary building

Following the proposed procedure (as demonstrated in the numerical study), system parameters of the assembled TMD and three-story benchmark building were extracted (Table 9). The conditions of both full measurement and single measurement were considered. Unlike the results of the numerical study, the $\hat{\omega}_s$ and $\hat{\xi}_s$ values were related to the selection of mode (*j*, *k*). Because the TMD was designed to tune the first mode of the building, and the average from (*j*, *k*) = (1, 2) and (3, 4) was taken, the results were as follows: $\hat{\omega}_s$ = 0.979 Hz and $\hat{\xi}_s$ = 8.65% in the full-measurement situation and $\hat{\omega}_s$ = 0.980 Hz and $\hat{\xi}_s$ = 8.95% in the single-measurement situation. The two identified $\hat{\omega}_s$ values were close to the assembled ω_s (1.028 Hz; 4.8% smaller), whereas the identified $\hat{\xi}_s$ values were slightly larger than the assembled ξ_s (7.41%). These differences were caused by many factors, such as modeling errors in the building–TMD system and regarding the five MTMD units as a whole. In addition, neglecting the weight of the springs, dampers, and rolling wheels in calculating the mass of an MTMD unit may have resulted in $\hat{\omega}_s$ slightly lower than ω_s. The extracted $\hat{\xi}_s$ being larger than the assembled ξ_s was attributed to the unexpected inherent friction of the MTMD device.

The final results of the modal frequencies and modal damping ratios of the benchmark building were determined from Table 9 according to the selection rule in section 3.3, for example $\hat{\omega}_0 = \{1.06\ \ 3.21\ \ 5.02\}$ Hz and $\hat{\xi}_0 = \{1.27\ \ 0.17\ \ 0.16\}$ % for the full-measurement situation and

$\hat{\omega}_0 = \{1.05\ 3.21\ 5.01\}$ Hz and $\hat{\xi}_0 = \{3.04\ 0.20\ 0.11\}$ % for the single-measurement situation. The extracted modal frequencies of both cases clearly agree with those of the bare-building test ($\omega_0 = \{1.08\ 3.24\ 5.03\}$ Hz) (Table 6). The slight discrepancy was due to the additional mass of the MTMD device (approximately 150 kg), which increased the mass of the third floor and thus reduced the three modal frequencies of the primary building. The extracted second and third modal damping ratios were accurate, and the error for $\hat{\xi}_{0_1}$ was relatively large but within an acceptable range.

The shaking-table experiment was repeated using the other two earthquake ground motions. All of the analysis results are illustrated in Figs. 7 (full measurement) and 8 (single measurement) and compared with those of the bare-building tests (labeled as "Reference"). The extracted parameters under the various ground-motion excitations were close, indicating that the proposed analysis procedure is applicable for evaluating the effectiveness of TMD control.

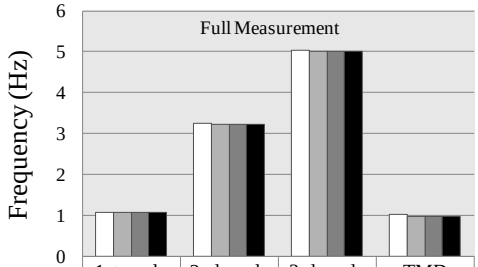

	1st mode	2nd mode	3rd mode	TMD
Reference	1.081	3.244	5.029	1.028
Chi-Chi	1.060	3.215	5.015	0.979
W.N.	1.065	3.214	5.016	0.973
EL Centro	1.063	3.214	5.016	0.975

(a) Extracted frequencies

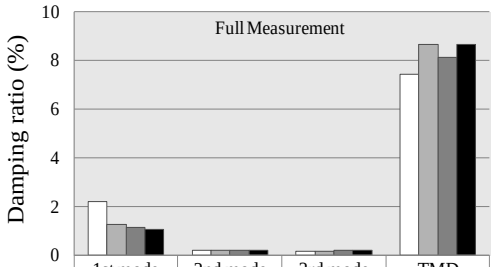

	1st mode	2nd mode	3rd mode	TMD
Reference	2.19	0.20	0.16	7.41
Chi-Chi	1.27	0.17	0.16	8.65
W.N.	1.14	0.19	0.18	8.12
EL Centro	1.06	0.19	0.17	8.67

(b) Extracted damping ratios

Fig. 7 Comparisons of the extracted parameters of the experimental building and TMD with the values of the bare-building tests under the full-measurement conditions of three ground motions

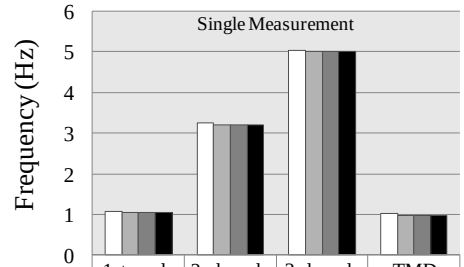

	1st mode	2nd mode	3rd mode	TMD
Reference	1.081	3.244	5.029	1.028
Chi-Chi	1.042	3.215	5.010	0.980
W.N.	1.046	3.214	5.014	0.974
EL Centro	1.045	3.215	5.013	0.976

(a) Extracted frequencies

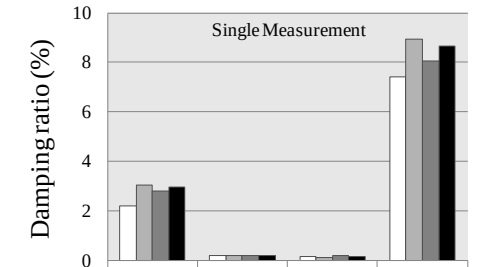

	1st mode	2nd mode	3rd mode	TMD
Reference	2.19	0.20	0.16	7.41
Chi-Chi	3.04	0.20	0.11	8.95
W.N.	2.79	0.20	0.17	8.07
EL_Centro	2.94	0.19	0.16	8.64

(b) Extracted damping ratios

Fig. 8 Comparisons of the extracted parameters of the experimental building and TMD with the values of the bare-building tests under the single-measurement conditions of three ground motions

Table 9 Extracted parameters of the assembled TMD and three-story benchmark building

Identified Parameters		(*j*, *k*)	Full measurement	Single Measurement
TMD	$\hat{\omega}_s$ (Hz)	(1, 2)	0.958	0.959
		(3, 4)	1.000	1.001
		(5, 6)	1.147	1.143
		(7, 8)	1.346	1.265
	$\hat{\xi}_s$ (%)	(1, 2)	9.13	9.30
		(3, 4)	8.76	8.80
		(5, 6)	8.84	8.19
		(7, 8)	7.46	8.07
Primary building (physical)	$\hat{c}_p$ (*k*N-sec/m)	(1, 2)	{9.126, 5.291, 4.719}	8.170
		(3, 4)	{3.408,3.946, -0.306}	5.750
		(5, 6)	{0.480, -0.580, 0.273}	1.421
		(7, 8)	{0.871, 0.072, 0.093}	1.249
	$\hat{k}_p$ (*k*N/m)	(1, 2)	{1372, 1321, 982}	691
		(3, 4)	{1393, 1352, 899}	827
		(5, 6)	{1642, 1497, 1488}	7201
		(7, 8)	{2582, 1632, 1867}	17488
Primary building (modal)	$\hat{\omega}_0$ (Hz)	(1, 2)	{**1.06**, 2.74, 4.11}	1.00
		(3, 4)	{**1.06**, 2.67, 4.11}	1.09
		(5, 6)	{1.16, **3.21**, 4.56}	3.21
		(7, 8)	{1.34, 3.74, **5.02**}	5.01
	$\hat{\xi}_0$ (%)	(1, 2)	{**1.82**, 4.63, 5.95}	3.70
		(3, 4)	{**0.72**, 0.50, 2.94}	2.38
		(5, 6)	{0.011, **0.17**, -0.16}	0.20
		(7, 8)	{0.070, 0.19, **0.16**}	0.11

5. Conclusions

In this study, an analysis procedure was developed for extracting the natural frequencies and damping ratios of a TMD and primary building based on the acceleration measurements of a combined building–TMD system. This procedure was first performed by identifying the eigenvalues and eigenvectors from the acceleration measurements of the building–TMD system. These complex eigenparameters were then used to calculate the respective parameters of the TMD and primary building by using the derived analytical formulas. Although the developed theory is based on the shear building assumption, the numerical-simulation results show that the extracted TMD parameters are influenced little by the building model, whereas the building parameters of different modes can be accurately extracted by selecting appropriately complex modes. Even under single-measurement conditions, the modal frequencies and damping ratios of the multiple modes can be obtained using the identified parameters of the "pseudoshear" building. The proposed procedure was further validated using the experimental data of shaking-table tests of a large-scale, three-story benchmark building equipped with an assembled five-unit TMD. Both full-measurement and single-measurement conditions were considered, and the proposed procedure can obtain accurate results. It is concluded that the proposed analysis procedure can be appropriately applied to the health monitoring of a building–TMD system and used for ensuring

TMD control performance (in particular, when a TMD is assembled simultaneously with building construction).

Acknowledgments

This work is supported by the Ministry of Science and Technology of the Republic of China (Taiwan) under grants no. 103-2625-M-178-001 and no. 95-2625-Z-005-009. These supports are greatly appreciated.

References

Alexander, N.A. and Schilder, F. (2009), "Exploring the performance of a nonlinear tuned mass damper", *J. Sound Vib.*, **319**(1-2), 445-462.

Almazán, J.L., Espinoza, G. and Aguirre, J.J. (2012), "Torsional balance of asymmetric structures by means of tuned mass dampers", *Eng. Struct.*, **42**, 308-328.

Bekdaş, G. and Nigdeli, S.M. (2011), "Estimating optimum parameters of tuned mass dampers using harmony search", *Eng. Struct.*, **33**, 2716-2723.

Bekdaş, G. and Nigdeli, S.M. (2013), "Mass ratio factor for optimum tuned mass damper strategies", *Int. J. Mech. Sci.*, **71**, 68-84.

Bakre, S.V. and Jangid, R.S. (2004), "Optimum multiple tuned mass dampers for base-excited damped main system", *Int. J. Struct. Stab. Dy.*, **4**(4), 527-542.

Bisegna, P. and Caruso, G. (2011), "Closed-form formulas for the optimal pole-based design of tuned mass dampers", *J. Sound Vib.*, **331**(10), 2291-2314.

Brock, J.E. (1946), "A note on the damped vibration absorber", *J. Appl. Mech. T. Am. Soc. Mech. E.*, **13**, A-284.

Brownjohn, J.M.W., Carden, E.P., Goddard, C.R. and Oudin, G. (2010), "Real-time performance monitoring of tuned mass damper system for a 183m reinforced concrete chimney", *J. Wind Eng. Ind. Aerod.*, **98**(3), 169-179.

Chakraborty, S. and Roy, B.K. (2011), "Reliability based optimum design of tuned mass damper in seismic vibration control of structures with bounded uncertain parameters", *Probabilist. Eng. Mech.*, **26**(2), 215-221.

Cheung Y. L. and Wong, W. O. (2011), "H-infinity optimization of a variant design of the dynamic vibration absorber-revisited and new results", *J. Sound Vib.*, **330**(16), 3901-3912.

Den Hartog, J.P. (1956), *Mechanical Vibrations*, McGraw-Hill, New York, U.S.A.

Farshidianfar, A. and Soheili, S. (2013), "Ant colony optimization of tuned mass dampers for earthquake oscillations of high-rise structures including soil–structure interaction", *Soil Dyn. Earthq. Eng.*, **51**, 14-22.

Frahm, H. (1911), *Device for damping vibrations of bodies*. U.S. Patent No. 989-958.

Greco, R. and Marano, G.C. (2013), "Optimum design of tuned mass dampers by displacement and energy perspectives", *Soil Dyn. Earthq. Eng.*, **49**, 243-253.

Hahnkamm, E. (1932), "Die dampfung von fundamentschwingungen bei veranderlicher erregerfrequenz", *Ingenieur Archiv*, **4**(2), 192-201.

Jangid, R.S. (1999), "Optimum multiple tuned mass dampers for base-excited undamped system", *Earthq. Eng. Struct. D.*, **28**(9), 1041-1049.

Jangn S.J., Brennan, M.J., Rustighi, E. and Jung, H.J. (2012), "A simple method for choosing the parameters of a two degree-of-freedom tuned vibration absorber", *J. Sound Vib.*, **331**(21), 4658-4667.

Juang, J.N. (1997), "System realization using information matrix", *J. Guid. Control Dynam.*, **21**(3), 492-500.

Kang, N., Kim, H., Choi, S., Jo, S., Hwang, J.S. and Yu, E. (2012), "Performance evaluation of TMD under

typhoon using system identification and inverse wind load estimation", *Comput. - Aided Civ. Inf.*, **27**(6), 455-473.
Kareem, A. and Kline, S. (1995), "Performance of multiple mass dampers under random loading", *J. Struct. Eng. - ASCE*, **121**(2), 348-361.
Kwok, K.C.S. (1984), "Damping increase in building with tuned mass damper", *J. Eng. Mech. - ASCE* , **110**(11), 1645-1649.
Li, C. (2000), "Performance of multiple tuned mass dampers for attenuating undesirable oscillators of structures under the ground acceleration", *Earthq. Eng. Struct. D.*, **29**(9), 1405-1421.
Li, C. and Zhu, B. (2006), "Estimating double tuned mass dampers for structures under ground acceleration using a novel optimum criterion", *J. Sound Vib.*, **298**(1-2), 280-297.
Li, Q.S., Zhi, L.H., Tuan, A.Y., Kao, C.S., Su, S.C. and Wu, C.F. (2011), "Dynamic behavior of Taipei 101 tower: field measurement and numerical analysis", *J. Struct. Eng.- ASCE*, **137**(1), 143-155.
Lin, C.C., Hu, C.M., Wang, J.F. and Hu, R.Y. (1994), "Vibration control effectiveness of passive tuned mass dampers", *J. Chin. Inst. Eng.*, **17**(3), 367-376.
Lin, C.C., Wang, C.E., Wu, H.W. and Wang, J.F. (2005), "On-line building damage assessment based on earthquake records", *Smart Mater. Struct.*, **14**(3), 137-153.
Lin, C.C., Wang, J.F. and Tsai, C.H. (2008), "Dynamic parameter identifications for irregular buildings considering soil-structure interaction effects", *Earthq. Spectra*, **24**(3), 641-666.
Lin, C.C., Wang, J.F., Lien, C.H., Chiang, H.W. and Lin, C.S. (2010), "Optimum design and experimental study of multiple tuned mass dampers with limited stroke", *Earthq. Eng. Struct. D.*, **39**(14), 1631-1651.
Lin, C.C. and Wang, J.F. (2012), *Optimal Design and Practical Considerations of Tuned Mass Dampers for Structural Control*, Design Optimization of Active and Passive Structural Control Systems, 126-149, IGI Global, Hershey, PA, USA.
Luft, R.W. (1979), "Optimal tuned mass dampers for buildings", *J. Struct. Div. - ASCE*, **105**(12), 2766-2772.
Marano, G.C. and Quaranta, G. (2009), "Robust optimum criteria for tuned mass dampers in fuzzy environments", *Appl. Soft Comput.*, **9**, 1232-1243.
Marano, G.C., Greco, R. and Chiaia, B. (2010a), "A comparison between different optimization criteria for tuned mass dampers design", *J. Sound Vib.*, **329**(23), 4880-4890.
Marano, G.C., Greco, R. and Sgobba, S. (2010b), "A comparison between different robust optimum design approaches: Application to tuned mass dampers", *Probabilist. Eng. Mech.*, **25**(1), 108-118.
McNamara, R.J. (1977), "Tuned mass dampers for buildings", *J. Struct. Div.- ASCE*, **103**(9), 1785-1798.
Mohtat, A. and Dehghan-Niri, E. (2011), "Generalized framework for robust design of tuned mass damper systems", *J. Sound Vib.*, **330**(5), 902-922.
Oka, S.Y., Song, J. and Park, K.S. (2009), "Development of optimal design formula for bi-tuned mass dampers using multi-objective optimization", *J. Sound Vib.*, **322**(1-2), 60-77.
Ormondroyd, J., and Den Hartog, J.P. (1928), "The theory of the dynamic vibration absorber", *J. Appl. Mech. T. Am. Soc. Mech. E.*, **50**, 9-22.
Park, J. and Reed, D. (2001), "Analysis of uniformly and linearly distributed mass dampers under harmonic and earthquake excitation", *Eng. Struct.*, **23**(7), 802-814.
Sgobba, S. and Marano, G.C. (2010), "Optimum design of linear tuned mass dampers for structures with nonlinear behavior", *Mech. Syst. Signal Pr.*, **24**(6), 1739-1755.
Shi, W., Shan, J. and Lu, X. (2012), "Modal identification of Shanghai World Financial Center both from free and ambient vibration response", *Eng. Struct.*, **36**, 14-26.
Steinbuch, R. (2011), "Bionic optimisation of the earthquake resistance of high buildings by tuned mass dampers", *J. Bionic Eng.*, **8**(3), 335-344.
Tigli, O.F. (2012), "Optimum vibration absorber (tuned mass damper) design for linear damped systems subjected to random loads", *J. Sound Vib.*, **331**(13), 3035-3049.
Ueng, J.M., Lin, C.C. and Wang, J.F. (2008), "Practical design issues of tuned mass dampers for torsionally coupled buildings under earthquake loadings", *Struct. Des. Tall Buil.*, **17**(1), 133-165.
Van Overschee, P. and De Moor, B. (2011), *Subspace Identification for Linear Systems: Theory – Implementation – Applications*, Springer, New York, NY, USA.

Viguie, R. and Kerschen, G. (2009), "Nonlinear vibration absorber coupled to a nonlinear primary system: A tuning methodology", *J. Sound Vib.*, **326**(3-5), 780-793.
Viguie R. and Kerschen, G. (2010), "On the functional form of a nonlinear vibration absorber", *J. Sound Vib.*, **329**(25), 5225-5232.
Villaverde, R. (1985), "Reduction seismic response with heavily-damped vibration absorbers", *Earthq. Eng. Struct. D.*, **13**(1), 33-42.
Wang J.F. and Lin, C.C. (2005), "Seismic performance of multiple tuned mass dampers for soil-irregular building interaction system", *Int. J. Solids Struct.*, **42**, 5536-5554.
Wang, J.F., Lin, C.C. and Lian, C.H. (2009). "Two-stage optimum design of tuned mass dampers with consideration of stroke", *Struct. Control Health.*, **16**(1), 55-72.
Wang, M., Zan, T., Yang, Y. and Fei, R. (2010), "Design and implementation of nonlinear TMD for chatter suppression: An application in turning processes", *Int. J. Mach. Tool. Manu.*, **50**(5), 474-479.
Warburton, G.B. (1982), "Optimum absorber parameters for various combinations of response and excitation parameters", *Earthq. Eng. Struct. D.*, **10**(3), 381-401.
Weber, B. and Feltrin, G. (2010), "Assessment of long-term behavior of tuned mass dampers by system identification", *Eng. Struct.*, **32**(11), 3670-3682.
Wirsching, P.H. and Campbell, G.W. (1973), "Minimal structural response under random excitation using the vibration absorber", *Earthq. Eng. Struct. D.*, **2**(4), 303-312.
Xu, K. and Igusa, T. (1992), "Dynamic characteristics of multiple substructures with closely spaced frequencies", *Earthq. Eng. Struct. D.*, **21**(12), 1059-1070.
Yu, H., Gillot, F. and Ichchou, M. (2013), "Reliability based robust design optimization for tuned mass damper in passive vibration control of deterministic/uncertain structures", *J. Sound Vib.*, **332**(9), 2222-2238.
Zilletti, M., Elliott, S.J. and Rustighi, E. (2012), "Optimisation of dynamic vibration absorbers to minimise kinetic energy and maximise internal power dissipation", *J. Sound Vib.*, **331**(18), 4093-4100.

CY